N_2 HOMO-1 orbital cross section revealed through high-order-harmonic generation

Jan Troß,[1,2] Xiaoming Ren,[1,*] Varun Makhija,[1,†] Sudipta Mondal,[1,‡] Vinod Kumarappan,[1] and Carlos A. Trallero-Herrero[1,§]
[1]*James R. Macdonald Laboratory, Department of Physics, Kansas State University, Manhattan, Kansas 66506, USA*
[2]*Institut für Kernphysik, Johann Wolfgang Goethe Universität Frankfurt, Max-von-Laue-Str. 1, 60438 Frankfurt, Germany*
(Received 13 January 2017; published 20 March 2017)

We measure multi-orbital contributions to high harmonic generation from aligned nitrogen. We show that the change in revival structure in the cutoff harmonics has a counterpart in the angular distribution when a lower-lying orbital contributes to the harmonic yield. This angular distribution is directly observed in the laboratory without any further deconvolution. Because of the high degree of alignment we are able to distinguish angular contributions of the highest occupied molecular orbital 1 (HOMO-1) orbital from angle-dependent spectroscopic features of the HOMO. In particular, we are able to make a direct comparison with the cross section of the HOMO-1 orbital in the extreme ultraviolet region.

DOI: 10.1103/PhysRevA.95.033419

I. INTRODUCTION

Higher-order-harmonic generation (HHG) [1–7] has been shown to be a powerful spectroscopic technique [8–12]. One benefit of HHG spectroscopy is that it can provide a coherent, time-dependent picture of molecular structure [13]. Because of the short driving pulses, it can be used to study field-free (free of the impulsive aligning field), fixed-in-space molecules [8,14] as well as excited electronic molecular states [15,16]. In particular, by using impulsive alignment [17] we are now able to access the molecular frame [18–21]. Impulsive alignment is achieved by creating a superposition of rotational quantum states which produces a time-dependent observable, revealed as a revival structure. Measurements like ionization [22,23], nonlinear optical methods [24,25], or HHG [11,26,27] are sensitive to this rotational wave packet and have been extensively used in the past [28,29]. Furthermore, recent studies have shown that changes in the revival dynamics can also occur when orbitals of different symmetry are involved [30–32]. Of particular relevance to this current article are previous results where the revival structure changes due to the influence of multiple orbitals when strong field ionization occurs from orbitals other than the highest occupied molecular orbital (HOMO). Multi-orbital contributions are more likely when the energy gap between the HOMO and lower orbitals is small compared with the ionization potential [30] and can change with the molecule's orientation with respect to the ionizing field [33]. Since ionization can arise from multiple orbitals, the time-dependent harmonic signal will change accordingly [30,33–36]. In this paper we measure multi-orbital contributions to the harmonic yield from aligned N_2. We show that the change in revival structure in the cutoff harmonics, when contributions from HOMO-1 are detected, has a counterpart in the angular distribution of harmonics at the time of maximum alignment. Furthermore, we can clearly distinguish two contributions to the angle-dependent harmonic yield. These distinguishable contributions are from the HOMO-1 orbital and the angle- and energy-dependent Cooper minimum of N_2 [18]. Finally, our results represent the first direct comparison of the HHG yield to photoionization cross section (PICS) for orbitals other than the HOMO.

II. EXPERIMENTAL SETUP

Our experimental setup is shown in Fig. 1. We use laser pulses from the Kansas Light Source (KLS), a home-built chirped-pulse-amplification laser with a central wavelength of 785 nm. The KLS produces 2 mJ of energy per pulse with a pulse duration of 30 fs full width half maximum (FWHM) at a repetition rate of 2 kHz. Pulses are split by a beam splitter into a probe arm and two pump arms. We use 40% of the 2 mJ for the probe, while the rest is split again to form two pulses for double-pulse alignment. In addition, we use a telescope in the pump arm, placed before the second beam splitter, to control the pump focus in our supersonic gas jet and to ensure that the pump beam focus is bigger than the probe focus. In our setup, all three pulses are noncollinear and thus overlap only at the focus of an $f = 400$ mm lens. To overlap all three pulses, we use a mask with holes for the pumps and a silver mirror that reflects the probe at 0° (see Ref. [18]). All beams in front of the focusing lens are aligned to be parallel so that they focus on the same spot. Still, temporal and spatial overlap is checked with a CCD camera and by monitoring the second-harmonic generation in a nonlinear crystal out of the vacuum chamber. With this optical arrangement we only probe the central part of our aligned ensemble. The two pumps travel different path lengths, so that one pump is delayed with respect to the other by 8.36 ps. While the first pump induces molecular alignment, the second pump kicks the molecule at the rising edge of the full revival due to the first pump and further increases the degree of alignment [37,38]. A kHz Even–Lavie valve [39] produces a rotationally cold (≈30 K) target by supersonic expansion of 70 bar of N_2 into the vacuum chamber; the interaction region is ≈1 mm away from the nozzle. The degree of alignment is quantified by the expectation value $\langle \cos^2\theta \rangle$, where θ is the angle between the molecular axis and laser polarization. By

*Permanent address: Institute for the Frontier of Attosecond Science and Technology, CREOL and Department of Physics, University of Central Florida, Orlando, FL 32816, USA.
†Current address: Department of Physics, University of Ottawa, Ottawa, ON K1N 6N5, Canada.
‡Current address: ELI-Hu Kft., Dugonics ter 13, H-6720 Szeged Hungary.
§trallero@phys.ksu.edu

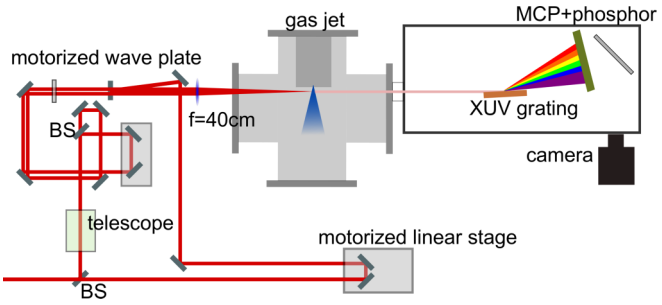

FIG. 1. Experimental setup; see text for details.

using two pumps and a cold target, we have demonstrated up to $\langle\cos^2\theta\rangle \approx 0.82$ for nitrogen [18]. In this manuscript, we present degrees of alignment of $\langle\cos^2\theta\rangle \approx 0.67$.

Harmonics are generated by the probe pulse, which is delayed with respect to both pumps by an automated delay stage. The entire harmonic spectrum is recorded as a function of delay between the first pump and probe pulses and as a function of the angle between pump and probe polarizations. We report the yield of each harmonic as the integral of the image in the spectral (horizontal) and spatial (vertical) direction. Because HHG is a macroscopic, coherent process and therefore very sensitive to the sample density, the laser focus is placed as close as possible to the nozzle. However, the throat of the conical nozzle is ≈6 mm away from the interaction region. This configuration ensures a cold target that still has sufficient density for the generation of harmonics. We estimate the molecular rotational temperature and the pumps' peak intensities and pulse durations by using the fitting procedure described in Ref. [18]. In short, we fit the entire revival structure by using the temperature of the gas ensemble and the laser parameters as fitting parameters. Following this method, we estimate the first pump to have an intensity of 33 TW/cm^2 and duration of 80 fs with the second one at 9 TW/cm^2 and 100 fs FWHM, while the temperature is estimated to be 30 K.

In this setup, the probe beam is clipped by a 10-mm-diameter iris before it is focused, and the gas jet is positioned 4 mm after the probe focus. Under these conditions we see long and short trajectories in the detector, which are distinguished by their spatial profile. The pulse duration of the probe was measured to be 33 fs (FWHM of the intensity), after compensating for all elements in the optical path. The probe intensity is calculated to be 190 TW/cm^2 when the beam is clipped by the 10 mm iris. A full probe pulse (no clip) had a calculated intensity of 360 TW/cm^2.

Generated harmonics pass through a 1-mm-wide slit and diffract from a grazing-incident grating with a groove density of 1200 groves/mm (Shimadzu 30-001). The frequency resolved harmonics are detected on a Chevron stack of microchannel plates, creating electron avalanches that in turn induce luminescence in a phosphor screen (Photonis APD 2 PS 75 mm). Finally, luminescence is collected by a Hamamatsu ORCA-Flash 2.8 camera, with a bit depth of 12 bits and a resolution of 1920 × 1440 pixels. Our final observable in all cases is the spectral and spatial integral of each individual harmonic, normalized to its isotropic value. The calibration of the spectrometer is done with emission lines of helium and neon [40] and also by following the grating equation.

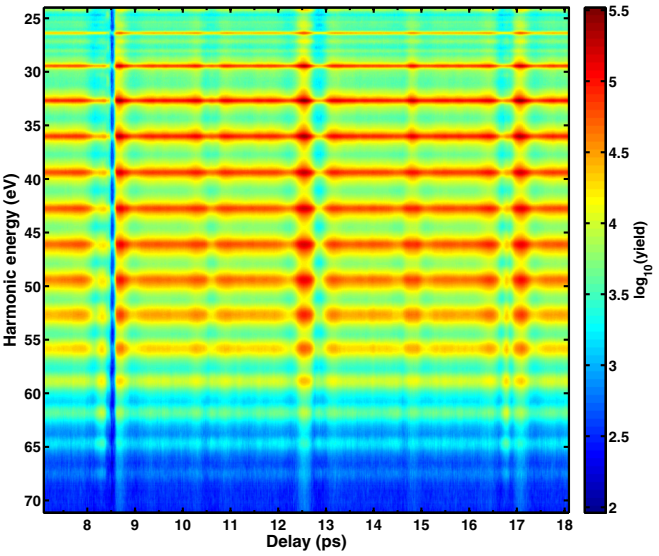

FIG. 2. Raw spectrum in logarithmic scale of harmonics generated from N_2 as a function of delay between the first pump and the probe and of the harmonic energy. The second pump is present at a delay of 8.36 ps with respect to the first pump. Strong features at times of alignment for all harmonics are visible. However, further features at times of anti-alignment before the full alignment revival (delay ≈16 ps) become more visible as the harmonic energy increases.

III. EXPERIMENTAL RESULTS

A. Time dependence

In Fig. 2 we show a delay-dependent harmonic spectrum on a logarithmic scale. We observe a pronounced plateau from 30 to 50 eV, with a rapid drop in yield for cutoff harmonics with energies larger than 55 eV. All harmonics show the expected full revival at ≈8.5 ps after the pump pulse, and the half and quarter revivals at corresponding times. However, in addition to the expected revival structure, harmonics higher than H29 (45 eV) show a distinctive peak at 16.78 ps, where the molecules are anti-aligned. A more detailed time-dependent picture is shown in Fig. 3 where we show the normalized H21, H23, H25, H31, H35, and H39 yields as a function of time in black. Normalization is done with respect to the isotropic values for each harmonic. The top panel of the figure shows the theoretically proposed $\langle\cos^4\theta\rangle(t)$ dependence with time for the harmonic yield from aligned N_2 [41]. All of the displayed scans start at 7.5 ps, just before the second pump pulse interacts with the molecular ensemble at 8.36 ps. Note that the vertical scale for each harmonic is different, as indicated in the axis legend, and the data points have been joined by lines to guide the eye. In the experimental analysis we use the 21st harmonic (H21) as a representation of plateau harmonics. H21 is in the known shape resonance $3\sigma_g \rightarrow k\sigma_u$ of N_2 for the HOMO at 30 eV [18,19]. It shows a $\langle\cos^4\theta\rangle$ behavior, the dominant term in the revival pattern for the HOMO of N_2 according to Refs. [41,42]. For harmonic 21, at ≈8.68 ps, the peak for prompt alignment can be seen, with half revivals and full revivals observed 4.5 and 8.4 ps later, respectively. H21 also exhibits quarter revivals present at 10.5 ps (≈2 ps after the second pump) and 1/8th revivals, present at ≈9.6 ps (≈1 ps after the second pump). Such high-order revivals in HHG from aligned nitrogen were

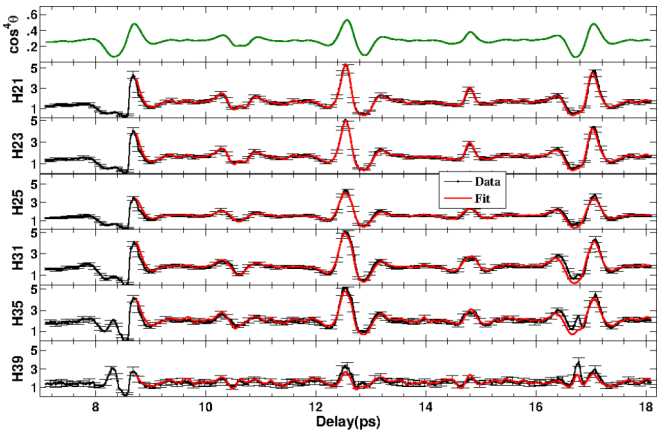

FIG. 3. Yield of harmonics H21, H23, H25, H31, H35, and H39 from N_2, normalized to the respective isotropic values, as a function of delay between the first pump and the probe in 20 fs steps (black). In all cases the second pump is at a delay of 8.36 ps with respect to the first pump. Harmonics 21 and 23 show the same behavior as our calculations of $\langle\cos^4\theta\rangle$, depicted in green (top panel). Harmonics 31 and higher show a peak at the anti-alignment dip (16.78 ps) in front of the full revival (17.04 ps). In particular, for harmonic 39 this peak becomes brighter than the full-revival peak. There are other smaller features in the delay scan of harmonic 39 that show a clear departure from the expected $\langle\cos^4\theta\rangle$. Also shown is the fitting using the procedure outlined in Ref. [18] (red). The error bars are the standard deviation from 18 averages, resulting in a standard error of the mean that is $\sqrt{18}$ smaller than the standard deviation.

first proposed in Ref. [41], measured first for other targets in Ref. [42], and recently observed by us experimentally in N_2 [18]. The shape of these high-order revivals can be explained by the angle- and energy-dependent (PICS) of the HOMO in N_2. Finally, by fitting the entire revival structure of H21 to our TDSE calculation, as described above and in Ref. [18], we estimate the degree of alignment to be $\langle\cos^2\theta\rangle \approx 0.67$.

By comparing the experimental yield of each harmonic with the top panel we can clearly see that harmonics between 30 and 40 eV exhibit a revival dynamics following the trends of $\langle\cos^4\theta\rangle(t)$. As we now look into the time-dependent behavior of spectral components at higher energies, we can see a strong feature arise at 16.78 ps. As previously reported for N_2 [30], multi-orbital contributions add additional features to the revival dynamics for harmonics in the spectral cutoff region. Such changes in the time-dependent revival structure are due to differences in the orbital geometry and are also present in our current data. This is most apparent at the anti-alignment feature at 16.78 ps where the molecular axis distribution of the molecule is an oblate structure with the major axis perpendicular to the polarization of the probe pulse. For this oblate angular distribution, on average, electron trajectories perpendicular to the molecular axis will contribute the most to HHG. Because the HOMO orbital has a node at 90° and thus a reduced ionization rate, we expect a dip at this particular delay. However, while we observe a minimum at 16.78 ps for H21, we observe a local maximum at the 16.78 ps delays for harmonics higher than H25. We are only able to explain the peak at 16.78 ps in H25 and higher orders by including contributions to the harmonic yield from electrons emitted perpendicular to the molecular axis from the HOMO-1 orbital. The HOMO-1 orbital has a maximum in its angular distribution perpendicular to the molecular axis and thus can explain a relative increase in the harmonic yield when the laser polarization and the molecular axis are at 90°. HOMO-1 is a π_u orbital and has a node at 0°. Contributions from lower orbitals to HHG are not limited to small fractions of the overall yield, however. For example, in harmonic 39, contributions from HOMO-1 to the revival structure are higher than any of the other revival peaks. That is, instead of an anti-alignment minimum at 16.78 ps, we observe a peak that is higher than the signal at the full revival at 17.04 ps. Furthermore, we can see a trace of HOMO-1 also in the anti-alignment dip after the half revival at 12.86 ps and at the anti-alignment dip of the quarter revival at 10.6 ps. Finally, we see a more complex behavior between quarter revivals (the signal level is well above the noise level of our detector). More specifically, for harmonic orders beyond 31, the 1/8th revivals at 9.6 and 13.6 ps have an opposite behavior compared with H21. This measurement shows the influence of lower orbitals on high-order revivals in high-order harmonics.

B. Angle dependence

To further investigate the contribution from HOMO-1 to the HHG process, and the interplay between angular distributions and revival structure, we measure harmonic yields as a function of the angle between pump and probe polarizations at the full revival of alignment after the second pump pulse. This corresponds to a maximum in the total harmonic yield at 17.04 ps. At this time, molecules are preferentially aligned parallel to the polarization of the harmonic generating pulse when the pump and probe polarizations are parallel. In Fig. 4, we plot the angle-dependent yield of harmonics 25–41 with $\langle\cos^2\theta\rangle \approx 0.67$ under the same macroscopic conditions as the data shown in Fig. 3. The yields are normalized to the isotropic yield for each harmonic. For harmonic orders below H25 the usual elongated yields are observed, with a maximum at 0° and a minimum at 90° between pump and probe.

The local minimum at 0° and 180° is due to the presence of the angle- and energy-dependent Cooper minimum in the N_2 HOMO [18]. While preserving features originating from the PICS of HOMO, we observe an additional feature at 90° and 270°. This feature becomes more pronounced with increasing harmonic order. The relative contribution of this new peak at 90° and 270° in the harmonic yield reaches, in the 39th harmonic, the same peak value as the yield at 30 degrees. This is in agreement with the fact that the revival structure for H39 in Fig. 3 has a global maximum at 16.78 ps rather than the expected maximum at 17.04 ps. We should emphasize that we are able to generate harmonics, with the field polarization at 90° with respect the molecular axis, with yields three times larger than the yield from an isotropic ensemble of N_2 molecules. This represents a large enhancement for harmonics in the cutoff.

Figure 5 compares the theoretical PICS for HOMO and HOMO-1 [43] with the experimental HHG signal as a function of angle for harmonics 35 to 41. In the figure we can observe that the HOMO PICS (dotted line) for harmonics 35 and 37 have a nonzero contribution at 90°. This nonzero contribution from the HOMO is due to the Cooper minimum [18] and is,

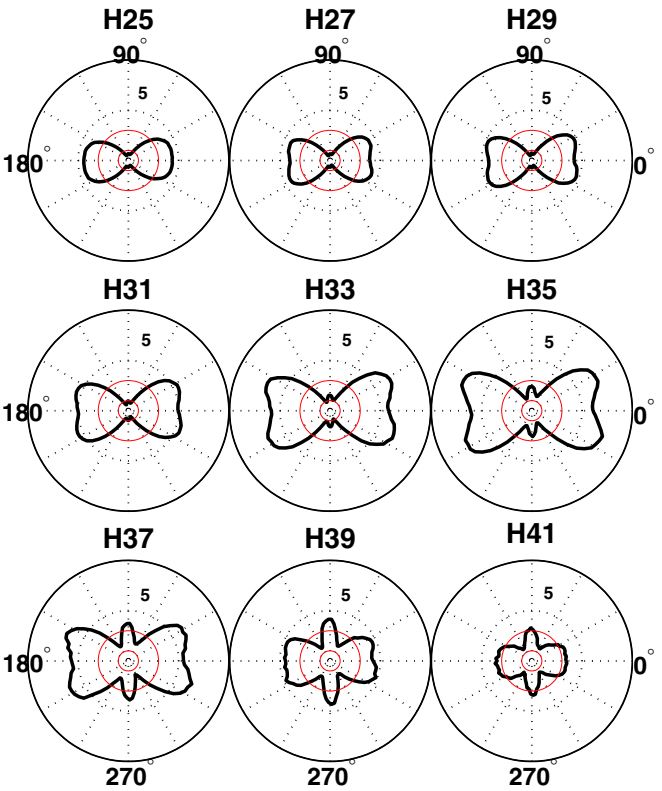

FIG. 4. Measured harmonic yield of individual harmonics as a function of angle between pump and probe at the full revival of 17.04 ps ($\langle\cos^2\theta\rangle \approx 0.67$). The experimental data were generated under the same conditions as presented in Fig. 3. Each harmonic yield is normalized to its corresponding isotropic value for an unaligned molecular ensemble. The red circles represent radial values of 1 and 3 units.

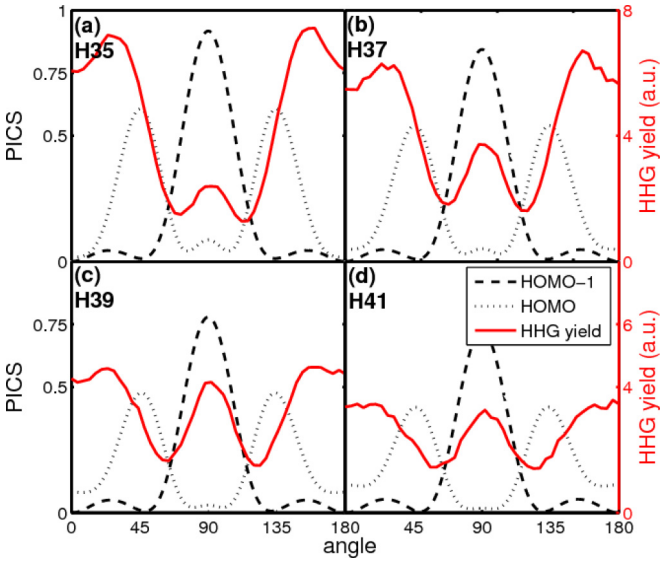

FIG. 5. A comparison between the experimental angle scans (solid red line) at the full revival of 17.04 ps and theoretical calculations of the photoionization cross sections of HOMO (dotted line) and HOMO-1 (dashed line) from Ref. [43]. The cross section is normalized to 1, while the experimental data are normalized to the isotropic harmonic yield. The dotted line of the PICS of HOMO shows a strong minimum at 0° and 180° that is due to the Cooper minimum in nitrogen. Without better alignment, this feature cannot be fully resolved. However, the feature at 90° can only be explained by the strong contribution from HOMO-1 to HHG (dashed line). As we then look at the experimental data as a function of harmonic order, the yield at 90° gets stronger as we increase the harmonic order, compared with 0° and 180°.

however, very small compared with the values close to 0°. For harmonics 39 and 41, the theoretical PICS of the HOMO predicts a zero contribution at 90°. On the other hand, from the experimental harmonic yield we observe that harmonics 35 and 37 have a local minimum at 0° and 180° and a global maximum at ≈30°, both of which are due to the Cooper minimum. However, the signal level at 0° and 180° is much higher than predicted by theory. Despite the fact that we do not observe zero signal for the Cooper minimum (0° and 180°), we do observe a fairly pronounced local peak at 90°. For harmonics 37, 39, and 41 this 90° peak is much larger than predicted by theory for the HOMO PICS at this angle. As the harmonics increase the signal at 90° becomes the largest compared with all other angles, even when the theoretical PICS predicts a zero value for the harmonics at this angle. Therefore, we are only able to explain the large contribution to the harmonic yield in H39 and H41 at 90° by adding a contribution from HOMO-1. Because the HHG yield is a convolution of ionization, electron wave-packet dynamics, and PICS, contributions from the HOMO-1 can arise due to ionization or due to structural factors in the PICS. This means that there could be either more ionization from the HOMO-1 than HOMO orbital and/or because at 90° the PICS for HOMO-1 is higher than the PICS for HOMO at these particular energies. While we do not know the relative contribution of ionization from HOMO-1, we can use the angular behavior of the harmonic yield and compare it to the PICS of HOMO and HOMO-1. This comparison in the theoretical calculations leads us to conclude that even for modest ionization yields we expect to see contributions from HOMO-1 for harmonics higher than H35.

IV. CONCLUSIONS

In this paper we present the first direct comparison of the HOMO-1 orbital in N_2 to PICS in the extreme ultraviolet region. In our opinion this represents a quantitative improvement compared with the detection of multi-orbital contributions. Our results open the possibility for future multi-orbital spectroscopy using HHG. To achieve a direct comparison, distinct contributions from the HOMO and HOMO-1 orbitals are detected in both the time-dependent revival structure and the angular distribution of the harmonic yields, with HOMO-1 contributions starting at harmonics as low as H29. We use two co-linear pumps and probe aligned N_2 molecules observing departures from the theoretically proposed $\langle\cos^4\theta\rangle(t)$ revival structure. For the angular measurements, we observe a contribution to the harmonic yield from HOMO-1 in the cutoff harmonics when the driver polarization and the molecular axis are at 90°. This signal at 90° is comparable in strength to 0° amplitudes that are expected when only the HOMO orbital is involved. For some harmonics, the 90° emission is

three times larger than emissions from an isotropic ensemble. Comparisons to theoretical calculations of the PICS confirm that the large yields in H39 and H41 at 90° confirm our assumptions of the involvement of the HOMO-1. However, the observed revival dynamics leaves a complete understanding of high harmonics generated from multiple orbitals still open. We propose that time-dependent phase measurements will help answering these questions.

Finally, unlike previous work [30,36], we are able to distinguish features in the harmonic yield arising from the shape resonance, Cooper minimum, and HOMO-1 orbital, thanks in part to our better degree of alignment than in those references. Furthermore, despite better alignment and higher peak intensities in the probe pulse, the results in Ref. [18] and [19,44] show no contribution from HOMO-1. This is in contradiction with microscopic arguments that, for stronger peak intensities, ionization from lower orbitals (and thus HHG) is more likely. Therefore, contributions from lower orbitals to HHG must be determined mainly by phase matching conditions that benefit higher-ionization-potential orbitals. In an upcoming presentation we will target the effect of phase matching and how it effects the relative contribution from HOMO-1 in N_2.

ACKNOWLEDGMENTS

The authors would like to thank C. Fehrenbach for input during the preparation of the manuscript. This work was supported by the Chemical Sciences, Geosciences, and Biosciences Division, Office of Basic Energy Sciences, Office of Science, U.S. Department of Energy (DOE) under Grant No. DE-FG02-86ER13491. We thank Cheng Jin and Anh–Thu Le for the fruitful discussions and access to the data first presented in Ref. [43].

[1] M. Lewenstein, P. Balcou, M. Y. Ivanov, A. L'Huillier, and P. B. Corkum, Phys. Rev. A **49**, 2117 (1994).
[2] P. B. Corkum, Phys. Rev. Lett. **71**, 1994 (1993).
[3] J. L. Krause, K. J. Schafer, and K. C. Kulander, Phys. Rev. Lett. **68**, 3535 (1992).
[4] A. McPherson, G. Gibson, H. Jara, U. Johann, T. S. Luk, I. McIntyre, K. Boyer, and C. K. Rhodes, J. Opt. Soc. Am. B **4**, 595 (1987).
[5] J. J. Macklin, J. D. Kmetec, and C. L. Gordon III, Phys. Rev. Lett. **70**, 766 (1993).
[6] A. L'Huillier and P. Balcou, Phys. Rev. Lett. **70**, 774 (1993).
[7] M. Ferray, A. l'Huillier, X. Li, L. Lompre, G. Mainfray, and C. Manus, J. Phys. B: At., Mol. Opt. Phys. **21**, L31 (1988).
[8] J. Itatani, J. Levesque, D. Zeidler, H. Niikura, H. Pépin, J.-C. Kieffer, P. B. Corkum, and D. M. Villeneuve, Nature (London) **432**, 867 (2004).
[9] M. Lein, N. Hay, R. Velotta, J. P. Marangos, and P. L. Knight, Phys. Rev. Lett. **88**, 183903 (2002).
[10] M. Lein, N. Hay, R. Velotta, J. P. Marangos, and P. L. Knight, Phys. Rev. A **66**, 023805 (2002).
[11] R. Velotta, N. Hay, M. B. Mason, M. Castillejo, and J. P. Marangos, Phys. Rev. Lett. **87**, 183901 (2001).
[12] T. Kanai, S. Minemoto, and H. Sakai, Nature (London) **435**, 470 (2005).
[13] S. Baker, J. S. Robinson, C. Haworth, H. Teng, R. Smith, C. Chirilă, M. Lein, J. Tisch, and J. Marangos, Science **312**, 424 (2006).
[14] W. Li, X. Zhou, R. Lock, S. Patchkovskii, A. Stolow, H. C. Kapteyn, and M. M. Murnane, Science **322**, 1207 (2008).
[15] H. Worner, J. Bertrand, D. Kartashov, P. Corkum, and D. Villeneuve, Nature (London) **466**, 604 (2010).
[16] J. P. Farrell, S. Petretti, J. Förster, B. K. McFarland, L. S. Spector, Y. V. Vanne, P. Decleva, P. H. Bucksbaum, A. Saenz, and M. Gühr, Phys. Rev. Lett. **107**, 083001 (2011).
[17] H. Stapelfeldt and T. Seideman, Rev. Mod. Phys. **75**, 543 (2003).
[18] X. Ren, V. Makhija, A.-T. Le, J. Troß, S. Mondal, C. Jin, V. Kumarappan, and C. Trallero-Herrero, Phys. Rev. A **88**, 043421 (2013).
[19] J. B. Bertrand, H. J. Wörner, P. Hockett, D. M. Villeneuve, and P. B. Corkum, Phys. Rev. Lett. **109**, 143001 (2012).
[20] K. Yoshii, G. Miyaji, and K. Miyazaki, Phys. Rev. Lett. **106**, 013904 (2011).
[21] R. de Nalda, E. Heesel, M. Lein, N. Hay, R. Velotta, E. Springate, M. Castillejo, and J. P. Marangos, Phys. Rev. A **69**, 031804 (2004).
[22] J. Mikosch, C. Z. Bisgaard, A. E. Boguslavskiy, I. Wilkinson, and A. Stolow, J. Chem. Phys. **139**, 024304 (2013).
[23] I. V. Litvinyuk, K. F. Lee, P. W. Dooley, D. M. Rayner, D. M. Villeneuve, and P. B. Corkum, Phys. Rev. Lett. **90**, 233003 (2003).
[24] V. Renard, M. Renard, A. Rouzée, S. Guérin, H.-R. Jauslin, B. Lavorel, and O. Faucher, Phys. Rev. A **70**, 033420 (2004).
[25] X. Ren, V. Makhija, and V. Kumarappan, Phys. Rev. A **85**, 033405 (2012).
[26] J. Levesque, Y. Mairesse, N. Dudovich, H. Pépin, J.-C. Kieffer, P. B. Corkum, and D. M. Villeneuve, Phys. Rev. Lett. **99**, 243001 (2007).
[27] P. Liu, P. Yu, Z. Zeng, H. Xiong, X. Ge, R. Li, and Z. Xu, Phys. Rev. A **78**, 015802 (2008).
[28] X. X. Zhou, X. M. Tong, Z. X. Zhao, and C. D. Lin, Phys. Rev. A **71**, 061801 (2005).
[29] X. X. Zhou, X. M. Tong, Z. X. Zhao, and C. D. Lin, Phys. Rev. A **72**, 033412 (2005).
[30] B. K. McFarland, J. P. Farrell, P. H. Bucksbaum, and M. Gühr, Science **322**, 1232 (2008).
[31] H. Soifer, P. Botheron, D. Shafir, A. Diner, O. Raz, B. D. Bruner, Y. Mairesse, B. Pons, and N. Dudovich, Phys. Rev. Lett. **105**, 143904 (2010).
[32] C. Vozzi, M. Negro, F. Calegari, G. Sansone, M. Nisoli, S. De Silvestri, and S. Stagira, Nat. Phys. **7**, 822 (2011).
[33] O. Smirnova, Y. Mairesse, S. Patchkovskii, N. Dudovich, D. Villeneuve, P. Corkum, and M. Y. Ivanov, Nature (London) **460**, 972 (2009).
[34] H. Akagi, T. Otobe, A. Staudte, A. Shiner, F. Turner, R. Dörner, D. Villeneuve, and P. Corkum, Science **325**, 1364 (2009).

[35] H. J. Worner, J. B. Bertrand, P. Hockett, P. B. Corkum, and D. M. Villeneuve, Phys. Rev. Lett. **104**, 233904 (2010).
[36] G. H. Lee, I. J. Kim, S. B. Park, T. K. Kim, Y. S. Lee, and C. H. Nam, J. Phys. B: At., Mol. Opt. Phys. **43**, 205602 (2010).
[37] C. Z. Bisgaard, S. S. Viftrup, and H. Stapelfeldt, Phys. Rev. A **73**, 053410 (2006).
[38] J. P. Cryan, P. H. Bucksbaum, and R. N. Coffee, Phys. Rev. A **80**, 063412 (2009).
[39] U. Even, J. Jortner, D. Noy, N. Lavie, and C. Cossart-Magos, J. Chem. Phys. **112**, 8068 (2000).
[40] J. Farrell, B. McFarland, P. Bucksbaum, and M. Gühr, Opt. Express **17**, 15134 (2009).
[41] S. Ramakrishna and T. Seideman, Phys. Rev. A **77**, 053411 (2008).
[42] R. M. Lock, S. Ramakrishna, X. Zhou, H. C. Kapteyn, M. M. Murnane, and T. Seideman, Phys. Rev. Lett. **108**, 133901 (2012).
[43] C. Jin, J. B. Bertrand, R. R. Lucchese, H. J. Wörner, P. B. Corkum, D. M. Villeneuve, A.-T. Le, and C. D. Lin, Phys. Rev. A **85**, 013405 (2012).
[44] R. Torres, T. Siegel, L. Brugnera, I. Procino, J. G. Underwood, C. Altucci, R. Velotta, E. Springate, C. Froud, I. Turcu *et al.*, Opt. Express **18**, 3174 (2010).